Generation of optical vortices by apodized photon sieves*

SUN Hai-bin (孙海滨)[1,2], **WANG Xing-hai** (王兴海)[1], **CHEN Jun** (陈君)[2], **and SUN Ping** (孙平)[1]**

1. School of Physics and Electronics, Shandong Normal University, Jinan 250014, China

2. College of Physics and Electronic Engineering, Taishan University, Tai'an 271000, China

(Received 9 December 2016; Revised 29 February 2016)

As a novel diffractive optical element, photon sieve has good focusing properties. We propose a method to verify the focusing properties by using apodized photon sieves. The apodized photon sieve is obtained by using a Gaussian window function to modulate the general photon sieve. Focusing properties of apodized photon sieve are studied by numerical simulations and experiments. It shows that photon sieves have good focusing ability, and the focusing ability of the photon sieve on the focal plane is stronger than that on other image planes. The experimental results also demonstrate that photon sieves can be used to generate optical vortices. The existence of optical vortices is confirmed by the formation of fork fringes. This apodized photon sieve is expected to have some practical applications in focusing analysis, optical imaging, and optical communication.

Document code: A **Article ID:** 1673-1905(2016)03-0237-4

DOI 10.1007/s11801-016-5254-8

As a novel diffractive optical element, photon sieve can focus soft X-rays to spot sizes smaller than the diameter of the smallest pinhole, and higher orders of diffraction and secondary maxima can be suppressed by several orders of magnitude[1]. Some theoretical and experimental researches related to photon sieves have been published, such as the designation of optical space telescope[2-5], the enhancement of weapons vision[6], the generation of hard X-rays vortex[7], the phase-contrast X-ray microscopy[8,9] and lithography[10,11].

Generation of high quality vortex beams is a very important issue in the research of optical vortex. The most used method is ultilizing computer-controlled liquid crystal spatial light modulator (LC-SLM)[12-15]. In this paper, we propose a new method that can be used to generate optical vorices by apodized photon sieves. The experimental results show that the experimental and theoretical intensity distributions concerning focusing ability have good agreement, and photon sieves can be used to generate optical vortices.

L. Kipp et al[1] analyzed the light amplitude using Fresnel-Kirchhoff diffraction integrals. The locations of the pinholes in the photon sieves satisfy the criterion for constructive interference, which requires that the optical path length from the source via the center of the holes to the focal point is an integral multiple of wavelength λ. Q. Cao et al[16] presented an individual far-field model for the focusing and imaging of the general pinhole photon sieves. Based on Rayleigh-Sommerfeld diffraction formula, Q. Cao et al[17] extended the individual far-field analytical model to the nonparaxial case of high-numerical-aperture photon sieves.

The success of photon sieves results from the following three factors[18], which are the large size of whole element, the smooth filtering for the population of pinholes, the different ratios d/w of different pinholes, where d is the diameter of an individual pinhole, and w is the width of the corresponding local zone. When the ratio values are d/w=1.53, 3.52, 5.51, 7.5, … and pinholes are centered on the bright zones, the intensity on the focal plane has a maximum value. On the other hand, when the ratio values are d/w=2.44, 4.47, 6.48, 8.48, …, the intensity on the focal plane has a minimum value.

It is known that when light passes through a rectangular-type transmission window, sidelobes are produced[19]. We utilize Gaussian function as a window apodization to modulate the pinhole density on each zone of the photon sieve, and obtain a smooth hologram of photon sieves. The equation of Gaussian apodization function is

$$G = \exp\left(-\frac{x^2}{2\sigma^2}\right), \tag{1}$$

where x is the optical path difference, and σ is the Gaussian standard deviation. An apodized photon sieve has fewer pinholes, i.e., there are 5 221 pinholes for the unapodized photon sieve and only 1 114 pinholes for the apodized photon sieve. By apodization, we can suppress the secondary maxima of the diffraction pattern, and obtain a low transmission.

* This work has been supported by the National Natural Science Foundation of China (No.61107012), and the Key Project of Science and Technology of Shandong Province (No.2012GGB01081).

** E-mail: sunpingmail@163.com

The designed photon sieve consists of a great number of pinholes whose locations and radii are properly chosen. The focal length and the diameter of the photon sieve are 260 mm and 5.8 mm, respectively. The pinholes of the photon sieve are centered on the bright zones. In a photon sieve with the ratio d/w of 1.53 as shown in Fig.1(a), there are 1 224 pinholes on the 12 bright zones, and the minimum and maximum radii of pinhole are 0.189 μm and 0.690 μm, respectively. Fig.1(b) shows an apodized photon sieve with 1 114 pinholes on the 25 bright zones.

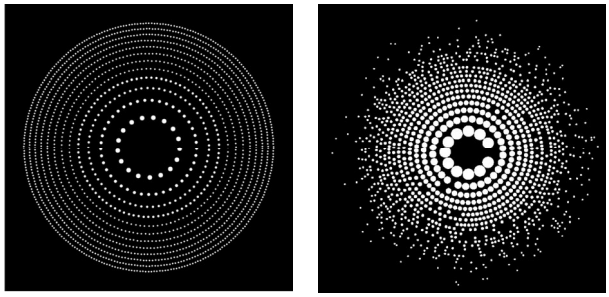

(a) (b)

Fig.1 Schematic diagrams of (a) a photon sieve and (b) an apodized photon sieve

According to the above theoretical models, we simulate the intensity distribution of a photon sieve which has 25 bright rings and 5 221 pinholes, and the simulated results are shown in Fig.2. In the simulation, the focal length of the photon sieve is 260 mm. Fig.2(a) and (b) show the three-dimensional (3D) and two-dimensional (2D) intensity distributions on the focal plane. Fig.2(c) and (d) show the 3D and 2D intensity distributions behind the focal plane of the photon sieve, and the distance between the photon sieve and image plane is 600 mm.

Fig.3 shows the schematic diagram of the experimental setup used in our method. A beam from a green single frequency continuous wave (CW) laser (532 nm) passes through a spatial filter, and is expanded by an expander lens, after which gets collimated and directed illumination onto a reflective spatial light modulator (SLM) screen (Holoeye, PLUTO) with a resolution of 1 920×1 080 pixels at a pixel size of 8 μm. A circular aperture is used to limit the size of the incident beam in order to avoid the beam spilling out the image array of the SLM. The SLM operates in a phase-only mode and is controlled by a computer. When a gray-scale image is displayed, the SLM will produce the same pattern and translate the gray level of the input image into corresponding phase value. A phase-only hologram of photon sieves is generated using Matlab software and displayed onto the SLM screen with an accuracy of 256 gray levels. In the reflected optical path, we place a high-speed charge coupled device (CCD) camera (DALSA Pantera TF 11M4) with a resolution of 4 008×2 672 pixels and pixel size of 9 μm×9 μm) on the focal plane of the photon sieve to capture the intensity distribution of the output optical field. The CCD is driven by a Coreco Imaging PC-DIG frame grabber. In the experiment, the focal length of the photon sieve is 260 mm.

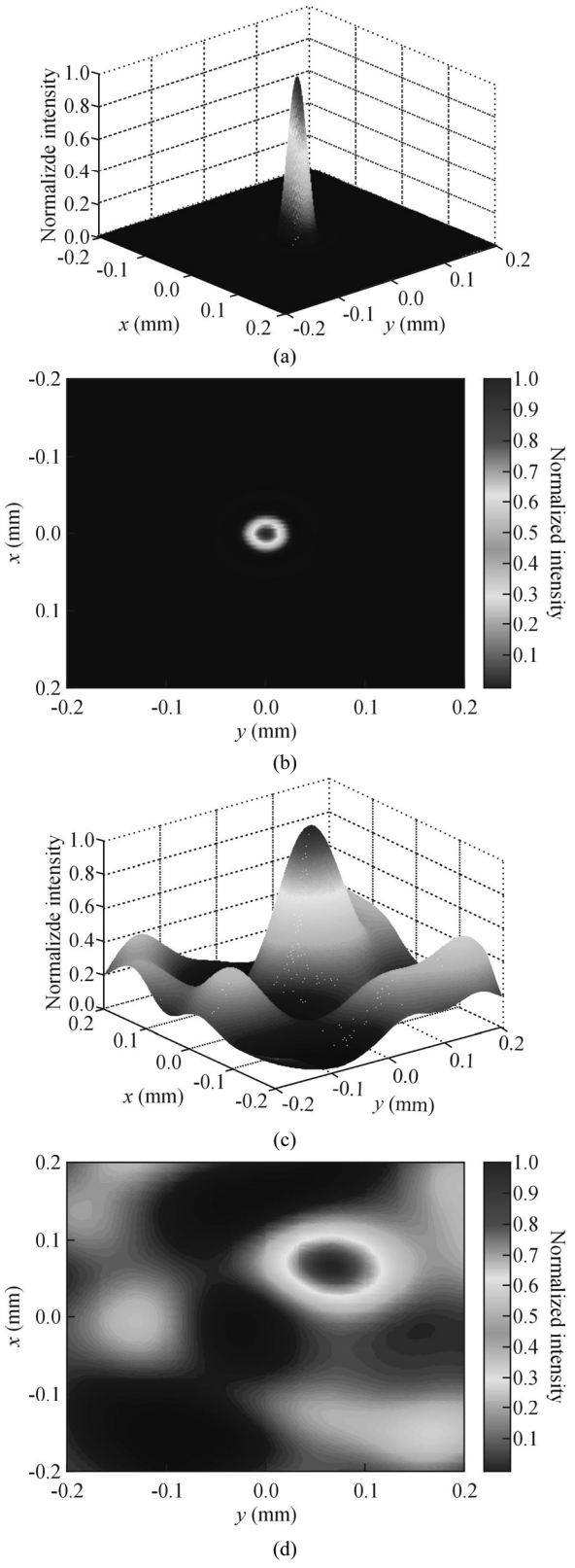

Fig.2 Simulation results of intensity distribution of photon sieve (a, b) on the focal plane and (c, d) behind the focal plane

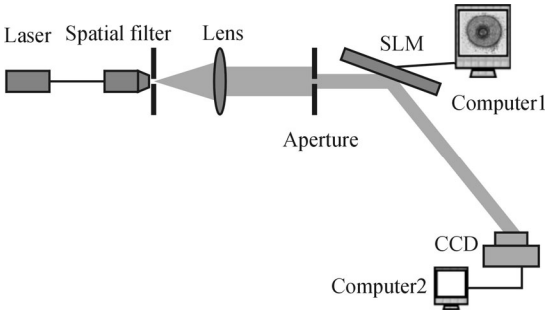

Fig.3 Schematic diagram of the experimental setup

When the CCD camera is placed on the focal plane and behind the focal plane of the photon sieve, the intensity distributions are obtained as shown in Fig.4. Fig.4(a) and (b) are the intensity distribution on the focal plane. Fig.4(c) and (d) are the intensity distribution behind the focal plane with the distance between LC-SLM and CCD of 400 mm. From these results, we can see that the intensity on the focal plane is much brighter than those on other image planes. We design another different apodized photon sieve in which pinholes are centered on the dark zones, and its hologram is also displayed onto the SLM. Fig.4(e) and (f) show the intensity distributions on the focal plane and behind the focal plane, respectively. From Fig.4(e) and (f), we can see that when pinholes are centered on opaque zones, the sign of the focal amplitude is reversed, and the result is in agreement with the theory. From the experimental results, we can conclude that the photon sieve has good focusing ability, and the focusing ability of the photon sieve on the focal plane is stronger than those on other image planes.

When an apodized photon sieve with 30 bright zones displays on the LC-SLM, the CCD camera captures the output optical field, as shown in Fig.5. Fig.5(a) and (d) show the experimental results on the focal plane and behind the focal plan with the distance between the LC-SLM and the CCD of 600 mm, respectively. Fig.5(b) and (e) are the enlarged amplitude distributions corresponding to Fig.5(a) and (d), respectively, and the dark spots marked by solid circles are optical vortex. Not all optical vortices are marked out. Fig.5(c) and (f) show the phase distributions of optical vortices on the focal plane and behind the focal plan, and the positions of optical vortices are marked by dark point. In Fig.5(c) and (f), the phase changing from $-\pi$ to π is represented by eight-interval color scale. The patterns indicate that the phase of the laser beam varies continuously from $-\pi$ to π. The patterns demonstrate that there are more optical vortices behind the focal plane than on the focal plane. The experimental results have good agreement with the numerical results obtained from Fig.2(c) and (d).

To determine the existence of the optical vortices, we display the output optical field's pattern of photon sieve on the screen of LC-SLM, as shown in Fig.5(a), and superimpose the output beam with the titled plane wave. The interference pattern of the two beams is captured by the CCD camera, which is shown in Fig.6. The split of the fringes can be regarded as the clue for the appearance of optical vortices, and these vortices are all first order vortices. From these experimental results of Figs.5 and 6, we can conclude that photon sieves can be used to generate optical vortices.

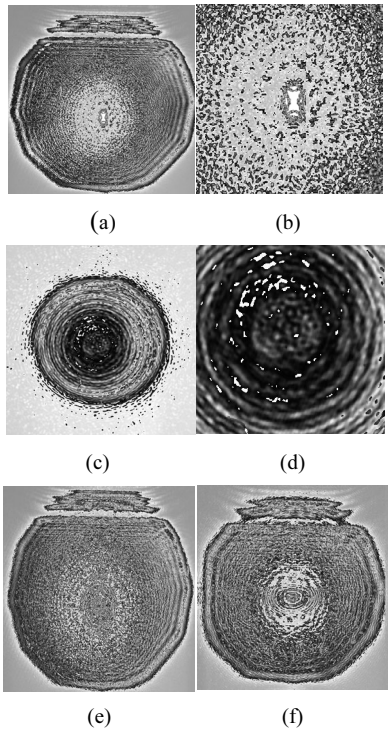

Fig.4 Experimental results of intensity distributions of the photon sieve (a) on the focal plane and (c) behind the focal plane; (b) The enlarged amplitude distributions of (a); (d) The enlarged amplitude distributions of (c); The intensity distributions of a photon sieve with pinholes centered on the dark zones (e) on the focal plane and (f) behind the focal plane

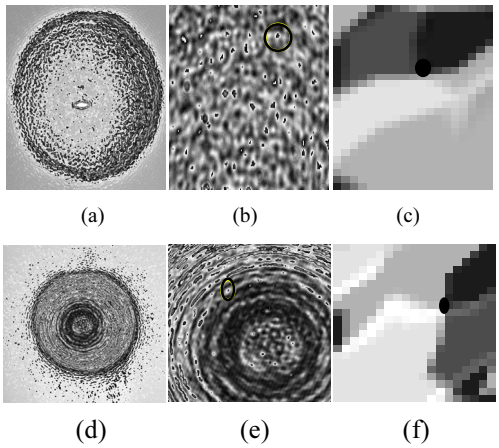

Fig.5 Experimental results of (a) intensity distribution, (b) enlarged amplitude distribution and (c) phase distribution of output beam on the focal plane; Experimental results of (d) intensity distribution, (e) enlarged amplitude distribution and (f) phase distribution of output beam behind the focal plan

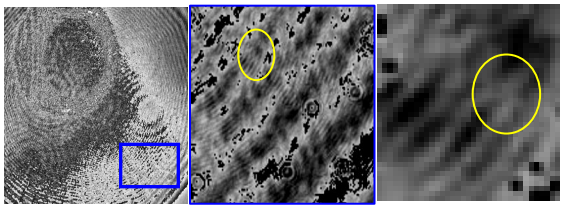

(a) (b) (c)

Fig.6 (a) Experimental pattern of interference of output beam from SLM with a titled plane beam; (b) Enlarged pattern and (c) fork pattern

To suppress the secondary maxima of the diffraction pattern, we utilize Gaussian functions to modulate the pinhole density of the photon sieve, and obtain the smooth hologram of the photon sieves. The experimental results demonstrate that an apodized photon sieve can be used to directly generate optical vortices. The proposed method is easily implemented using a traditional optical setup, and does not need a complicated experiment design. This apodized photon sieve is useful for focusing analysis, optical imaging, optical encoding and optical communication.

References

[1] L. Kipp, M. Skibowski, R .L. Johnson, R. Berndt, R. Adelung, S. Harm and R. Seemann, Nature **414**, 184 (2001).

[2] G. Andersen and D. Tullson, Applied Optic **46**, 3706 (2007).

[3] G. Andersen, Applied Optics **49**, 6391 (2010).

[4] O. Asmolova, G. Andersen, M. E. Dearborn, M. G. McHarg, T. Quiller and T. Murphey, Processings of SPIE **8739**, 87390C (2013).

[5] J. M. Davila, Processings of SPIE **8148**, 81480O (2011).

[6] K. Kincade, Laser Focus World **40**, 34 (2004).

[7] C. Xie, X. Zhu, L. Shi and M. Liu, Optics Letters **35**, 1765 (2010).

[8] G. Cheng, C. Hu, P. Xu and T. Xing, Optics Letters **35**, 3610 (2010).

[9] C. Xie, X. Zhu, H. Li, L. Shi, Y. Hua and M. Liu, Optics Letters **37**, 749 (2012).

[10] R. Menon, D. Gil, G. Barbastathis and H. I. Smith, Journal of the Optical Society of America A **22**, 342 (2005).

[11] M. Cheng and C. Zhou, Journal of Vacuum Science & Technology B **29**, 041002 (2011).

[12] N. Londoño, E. Rueda, J. A. Gómez and A. Lencina, Applied Optics **54**, 796 (2015).

[13] A. Kapoor, M. Kumar, P. Senthilkumaran and J. Joseph, Optics Communications 365, **99** (2016).

[14] ZOU Li-min, PANG Ming-shu, ZHOU Meng-jiao, WANG Bao-kai and TAN Jiu-bin, Journal of Optoelectronics·Laser **25**, 2329 (2014). (in Chinese)

[15] LIU Ji-lin, HUANG Hui-ling, CHEN Zi-yang, PU Ji-xiong and LIN Zhi-li, Journal of Optoelectronics·Laser **26**, 1626 (2015). (in Chinese)

[16] Q. Cao and J. Jahns, Journal of the Optical Society of America A **19**, 2387 (2002).

[17] Q. Cao and J. Jahns, Journal of the Optical Society of America A **20**, 1005 (2003).

[18] Q. Cao and J. Jahns, Journal of the Optical Society of America A **20**, 1576 (2003).

[19] C. Zhou, X. Dong, L. Shi, C. Wang and C. Du, Applied Optics **48**, 1619 (2009).